Experimental Study of an Axisymmetric Cavitylike Flow

Keith Koenig*
Mississippi State University, Starkville, Mississippi
and
Larry D. Vincent†
Lockheed-Georgia Company, Marietta, Georgia
and
Lisa W. Griffin‡
Lockheed Missile and Space Company, Huntsville, Alabama

An experimental investigation of a subsonic, axisymmetric, cavitylike flow has been performed. The configuration consists of a plane-nosed circular cylinder axially aligned with the flow, on which is affixed a thin concentric ring with variable diameter and axial location. The cavitylike region between the cylinder face and ring is documented by surface mean pressure distributions and surface flow visualization. Three distinct flow modes develop as the ring diameter and axial location are varied. Two modes resemble open and closed modes of conventional rectangular cavities. The third mode, when the ring is very close to the cylinder face, resembles flow past a circular disk. The pressure distributions and the lengths of the various separated regions depend on the ring height above the cylinder surface and the distance between the cylinder face and the ring, a consequence of the dominating influence of the cylinder face and the ring in different regions of the flow.

Nomenclature

C_p = pressure coefficient based on freestream conditions
d_1 = ring outer diameter
d_2 = cylinder diameter
h = height of ring above cylinder surface, $1/2(d_1 - d_2)$
ℓ, l = forebody length, distance from cylinder face to ring
L = total cylinder length
M = Mach number
r = radius, along cylinder face
r_2 = cylinder radius
x = axial position measured from the cylinder face
x_{rcyl} = distance to reattachment for cylinder alone
x_{r1} = distance to reattachment in the forebody region
x_{r2} = distance to reattachment downstream of the ring
x_s = distance to separation ahead of the ring
δ^* = displacement thickness
θ = momentum thickness

Presented as Paper 86-1067 at the AIAA/ASME Fourth Fluid Mechanics, Plasma Dynamics and Lasers Conference, Atlanta, GA, May 12–14, 1986; received May 19, 1986; revision received March 18, 1987.

*Associate Professor, Aerospace Engineering. Member AIAA.
†Associate Aircraft Engineer, Engineering Flight Test and Evaluation. Member AIAA.
‡Associate Engineer, Senior, Computational Fluid Mechanics, Member AIAA.

Introduction

THE usual notion of a cavity is some sort of cutout or depression in a surface past which a fluid flows. Separated (i.e., reverse flowing) fluid occupies some, if not all, of the cavity. There are actually many situations that possess cavitylike flows. The essential requirement is that there be two tandem bodies, or portions of a body, in a flow such that the leading body (or portion) produces separated flow downstream of itself, while the trailing body causes separation to occur on or upstream of itself. The leading and trailing bodies are then analogous to the upstream and downstream walls of a traditional rectangular cavity, respectively.

Cavities and cavitylike flows that are essentially two-dimensional have been studied in some detail, and the literature contains a reasonably complete collection of data regarding two-dimensional cavity flow. There are also a number of investigations of three-dimensional cavities. References 1–9 represent some of the more important fluid mechanic investigations of two- and three-dimensional cavities. The works of Roshko[1] and Charwat et al.[2] are particularly significant in defining the essential character of the flow. Axisymmetric cavities, on the other hand, have received comparatively little attention so that even such basic cavity properties as mean surface pressure distributions and critical cavity lengths are difficult to find in the open literature. The studies in Refs. 9–13 represent much of the available data on axisymmetric cavities.

The present investigation has been undertaken to supply data on some of the basic fluid mechanic properties of an axisymmetric cavitylike flow. In this study, a flat-faced circular cylinder is axially aligned with a flow and on the cylinder is flush-mounted a thin, concentric ring; the ring diameter and axial location are adjustable. This configuration resembles a cavity in that the cylinder face (the leading body) produces separated flow downstream of its edge or corner, whereas the ring (the trailing body) causes flow to separate ahead. The cylinder and ring thus essentially form an axisymmetric cavity. This particular arrangement was chosen for study primarily because it provides a mechanically simple way to vary the cavity geometry (due to the ease with which the ring can be changed and moved) while still accurately repre-

senting the more important fluid mechanic properties of cavities. The cylinder/ring also serves as a model for various practical situations. In particular, the cylinder/ring flow is much like the flow past certain drag reduction devices such as the cab-mounted air deflectors on large trucks[14] and the nose spike on the Trident missile.[15] These devices produce roughly axisymmetric cavitylike flow[16] so that the cylinder/ring is a representation of these as well.

This paper describes an experimental investigation of the cylinder/ring immersed in an essentially incompressible freestream. The focus of this work is the cavitylike nature of the flow as depicted by mean surface pressure distributions and surface flow patterns. Particular emphasis is placed on identifying the characteristic flow modes and associated critical geometries that develop as the length-to-height ratio of the cylinder/ring cavity is varied.

Experimental Details

The experiments were performed in a subsonic closed-circuit wind tunnel, with an octagonal test section of 1.01 m^2 area. The freestream turbulence level in this tunnel is approximately 0.5% at a freestream velocity of 36 m/s. The downstream end of the test section is vented to the atmosphere. All results reported here are for a freestream velocity of 36.6 m/s, corresponding to a freestream Mach number of 0.11, and the Reynolds number based on the cylinder diameter is 1.9×10^5.

Two models were constructed for these experiments, one for measurements of surface pressure distributions and a second for surface flow visualization observations. Figure 1 presents a schematic view of the model with various lengths defined. The mainbody of each model is a machined aluminum tube 920 mm long and 76.2 mm in diameter. Each model has a face plate and a base plate that were machined flat with sharp edge (or shoulder) radii. Three rings were made for these experiments. Each ring is 0.97 mm thick with an inner diameter of nominally 76.2 mm to give a snug fit on the mainbody, and the outer diameter of each ring is 102 mm, 127 mm, and 152 mm, respectively. The mainbody (for pressure measure-ments) is instrumented with 46 static pressure ports, 0.9 mm inner diameter, which are connected via 1.67 m of plastic tubing to a rotating valve and then to a strain gage transducer. The transducer output is digitally sampled by a Hewlett-Packard 3052A Data Acquisition System at a rate of 4 sample/second for 5 s for each port. The pressure taps are located along three rays of the cylinder surface, separated by 120 deg, to check for flow asymmetry. Six steel wires, 0.38 mm in diameter, support the mainbody in the tunnel. The mainbody plus support wires create a solid blockage of only 0.5% of the tunnel cross-sectional area, whereas with the largest ring in place the solid blockage is 1.8%.

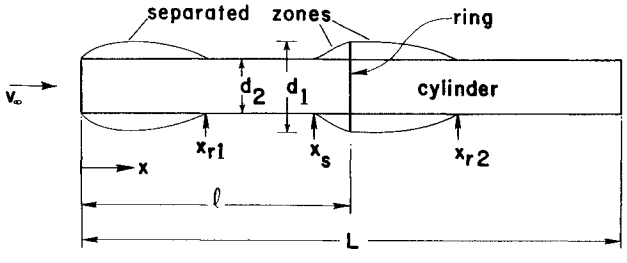

Fig. 1 Cylinder/ring configuration and flowfield.

The pressure coefficient (C_p) at each measurement location is based on freestream static and stagnation pressure as measured in the plane containing the mainbody face. Experimental uncertainty in the pressure coefficient due to slight flow asymmetry and unsteadiness is $C_p \pm 0.015$ for a freestream velocity of 36.6 m/s. No corrections to the pressure coefficients reported here have been made for solid blockage or the tunnel longitudinal pressure gradient. Further details regarding the measurement procedure may be found in Ref. 17.

Surface flow patterns were observed in these experiments using tuft and oil flow techniques.[18] The tufts were 8 mm long cotton thread taped to the surface. For the oil flow observations, a mixture of Crisco oil and powdered zinc oxide (four parts by volume Crisco, one part by volume zinc oxide) was dotted onto the model surface, along the upper axial generatrix. Dots of oil along the upper generatrix are less susceptible to being pulled over the side of the model by gravity and also produce generally clear indications of the separation and reattachment locations. With a freestream velocity of 36 m/s, the oil flow patterns developed in approximately three minutes. The surface flow patterns are the primary source for determining the points of separation and reattachment, and the mode of the flow. Nomenclature for distances to the separation and reattachment points is defined in Fig. 1.

Pressure Distributions

The reference geometry for this experiment is the plane-nose cylinder without a ring. This geometry is characterized by a single separated zone that originates at the face corner and terminates with reattachment onto the cylinder side. In the present experiment, oil flow indicated that reattachment occurs about 1.7 diameters downstream of the cylinder face, which agrees with previous investigations.[13,18]

Pressure distributions along the side of the cylinder without a ring, as measured in the present work, are presented in Fig. 2 together with results from Ota[19] and Stanbrook[20] (at a freestream Mach number of 0.7) for comparison. The pressure is quite low at separation and within the first portion of the separated zone with a very rapid recompression to reattach-

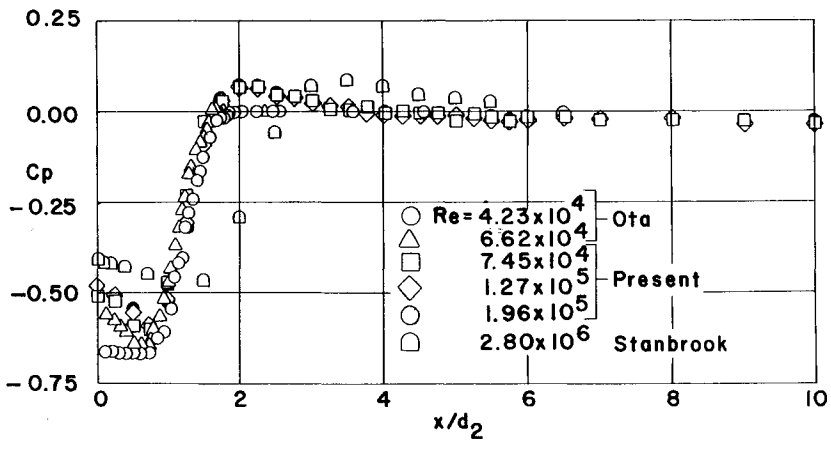

Fig. 2 Axial pressure distribution, the cylinder alone.

ment. The present results and those of Stanbrook show an overshoot and gradual relaxation to freestream pressure; these features are nearly absent in the distributions observed by Ota, however. There appears to be sensitivity to Reynolds number in the pressure at separation and at the recompression maximum, but much less sensitivity within the bulk of the separated zone. Compressibility has a large influence on the distribution as shown by the results of Stanbrook for a subcritical flow; the critical Mach number for this geometry is 0.8.[20]

A ring mounted on the cylinder side far downstream from the cylinder face produces a disturbance in the pressure as shown in Fig. 3. (For this figure, the rings are all mounted at the same axial location, $l/d_2 = 11.67$.) The upstream extent of the ring influence appears to be approximately five cylinder diameters essentially independent of the ring diameter studied here. However, the magnitude of the pressure rise does increase as the ring diameter, or equivalently, as the ring height above the cylinder surface increases.

The pressure distributions in Fig. 3 represent what might be called the closed-cavity mode (as defined by Charwat et al.[2]) for cylinder/ring configurations. This is seen by comparing the cylinder/ring pressures to those for two closed cavities, one from Roshko[1] (nominally two-dimensional, $M = 0.07$) and a second from Johannsen[10] (axisymmetric, $M = 1.97$), also shown in Fig. 3. There is an initial separation at the cylinder face with a corresponding pressure coefficient that has a relatively low, negative value. A rapid recompression leads to reattachment onto the cylinder side. Downstream of this reattachment the pressure is roughly constant for some distance, in what is commonly referred to as the plateau region. The flow then experiences a second pressure rise as it encounters the influence of the ring, and eventually, a second separation occurs in the midst of the adverse pressure gradient upstream of the ring. A second reattachment occurs somewhere on the ring. The cylinder/ring flow is clearly quite similar to a closed cavity with respect to the flow processes that occur and the qualitative shape of the pressure distributions.

As the ring location is moved upstream toward the cylinder face, pressure distributions such as those presented in Fig. 4 develop along the side of the cylinder. The distributions in Fig. 4 are only for the cylinder surface upstream of the ring, that is for x from 0 to l, which shall be referred to as the cylinder/ring forebody.

If we refer to Fig. 4, progressively decreasing the forebody length for a given ring brings about several changes to the pressure distributions. The pressure level at separation becomes more positive, the locations of the pressure minimum and the beginning of the pressure plateau move downstream relative to the forebody length, and the pressure overshoot (just past reattachment) and the plateau gradually disappear. The forebody length at which the plateau disappears (here, somewhere between $l/h = 10$ and 8) signifies a transition from

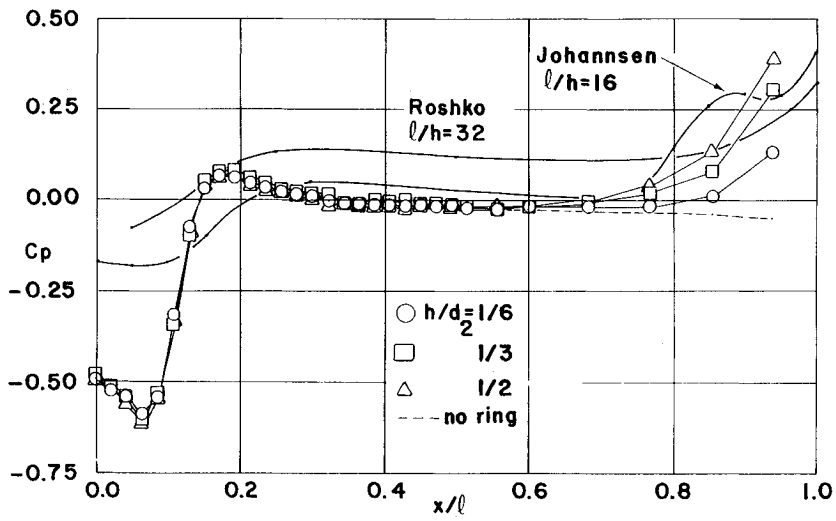

Fig. 3 Effect of a ring far downstream on forebody pressure distribution ($\ell/d_2 = 11.67$).

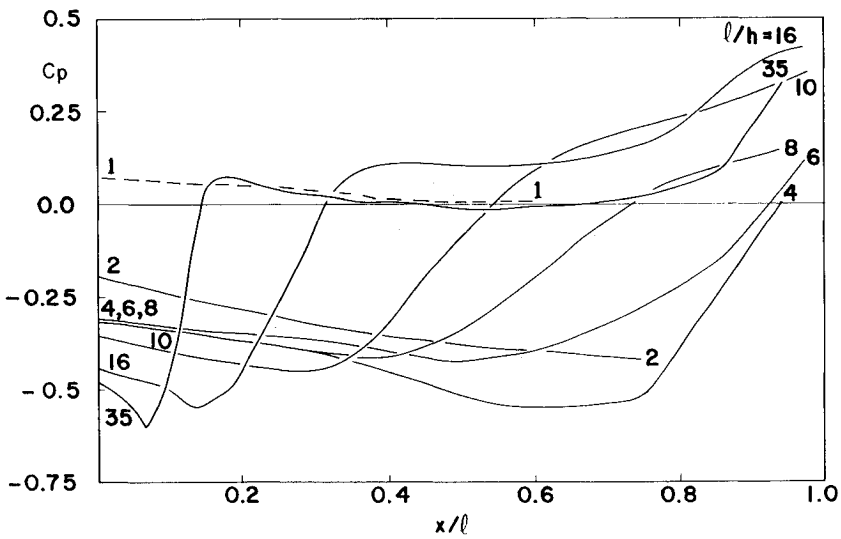

Fig. 4 Representative forebody pressure distributions, $h/d_2 = 1/3$.

the closed cavitylike flow that occurs for relatively long forebodies to a new flow mode that closely resembles an open cavity[2] flow. The characteristics of the open flow are a broad, relatively shallow pressure minimum followed by a continuous pressure rise to reattachment somewhere on the ring. For a conventional rectangular cavity, the separation streamline from the upstream cavity wall completely spans the cavity and reattaches onto the downstream wall so that the cavity is filled with one predominant separated zone. With the cylinder/ring, the flow is similar, separating at the cylinder corner and reattaching onto the ring with the forebody immersed in a single separated zone. For the sake of clarity, comparison pressure distributions for open two-dimensional cavities are not shown, but Refs. 1–8 present many examples much like those in Fig. 4 for $l/h = 4$ and 6. When the forebody length becomes quite short, such as $l/h = 1$ in Fig. 4, the pressure coefficient becomes positive even immediately downstream of the cylinder corner. (The curves for $l/h = 1$ and 2 do not extend completely to $x/l = 1$ because the tap locations were fixed and, therefore, taps were not available proportionally throughout all forebodies.) From results to be presented in a later figure, this type of distribution represents a third mode in which the ring appears to the external flow more as an extension of the cylinder face rather than a downstream obstacle.

The entire set of pressure distributions obtained during this work for each of the three rings is presented in Fig. 5 in order to completely define the mean surface conditions as a function of model geometry. Figure 5 demonstrates that the trends observed in Fig. 4 occur for all three rings. In particular, the three flow modes—closed cavity, open cavity, and the short forebody mode—all appear. There are not any significant differences in the closed cavity modes for the three ring heights except in the maximum pressure obtained as x/l approaches one. For the open cavity and short forebody modes, the pressure level along the entire forebody becomes increasingly more positive as the ring height increases. For the shortest forebody length, only one point for each ring is plotted, but this indicates the very high value of pressure that occurs.

Additional insight into the significance of the geometrical parameters (cylinder diameter, ring height, and forebody length) can be obtained by replotting some of the pressure distributions in Fig. 5 with different reference lengths. First, Fig. 6 compares the three rings at the same forebody cavity aspect ratio (l/h) with forebody length as the abscissa reference. Examples of a closed ($l/h = 20$) and an open flow ($l/h = 4$) are shown. Although the curve shapes are similar, there are large differences in the locations of various features and in the pressure levels, indicating that the forebody cavity aspect ratio alone is not sufficient to define the flow. If axial position is referenced to the cylinder diameter, as in Fig. 7, then the closed flow curves collapse to essentially the same curve up until the reattachment pressure maximum and then differ beyond that location. The upstream separated zone in the closed mode is, therefore, primarily dependent on the cylinder diameter, whereas the reattached and separating flow depends on both the forebody cavity aspect ratio and the cylinder diameter. From Figs. 6 and 7, the open mode depends on l/h and h/d_2. Similar conclusions can be drawn from Fig. 8 where fixed values of forebody length, closed and open modes, are compared. Again, the upstream closed mode separated zone depends primarily on l/d_2, whereas the other zones depend on both l/d_2 and l/h.

Some interpretation of the observations made regarding Figs. 6–8 is possible with help from the measurements of Ota[19] on a plane-nosed cylinder alone. Ota observed that the separation zone from the cylinder face edge had a maximum height normal to the cylinder of approximately $0.25d_2$ and extended downstream approximately $1.6d_2$. The reattaching flow had essentially a constant value of momentum thickness, $\theta \doteq 0.11d_2$. The displacement thickness, δ^*, dropped from $0.25d_2$ at reattachment to $0.15d_2$ at about three diameters downstream of the cylinder face, beyond which δ^* remained constant. The smallest ring here has a height ($h/d_2 = 0.16$) on the same order as the reattached boundary-layer integral thicknesses and smaller than the separation zone height. The

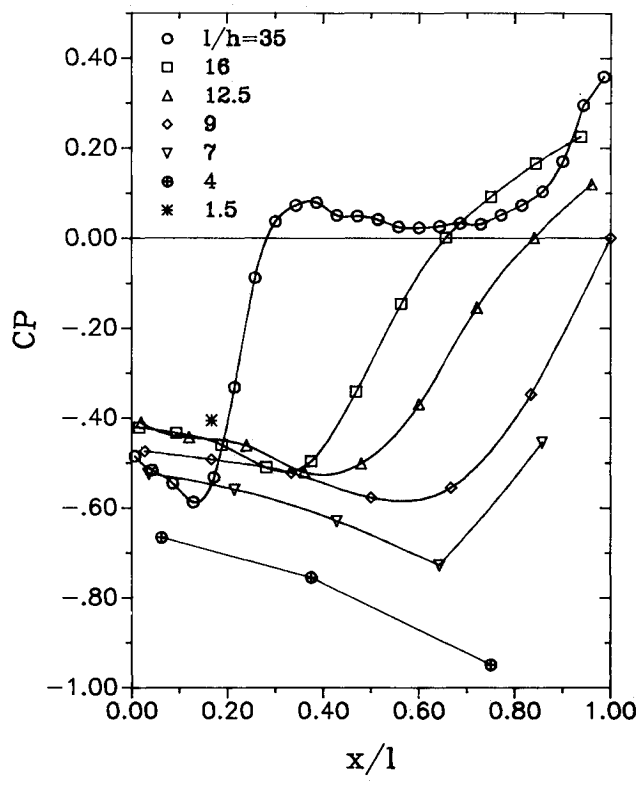

Fig. 5a Forebody pressure distributions, $h/d_2 = 1/6$.

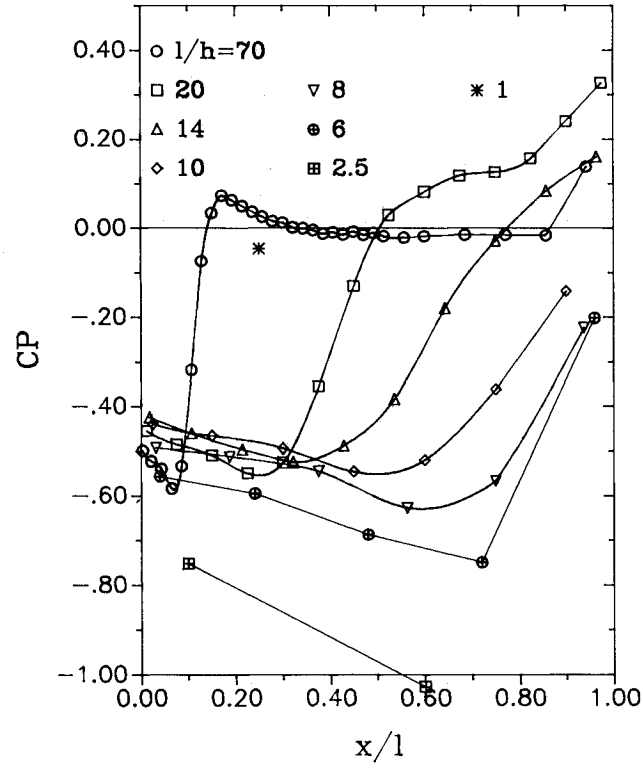

Fig. 5b Forebody pressure distributions, $h/d_2 = 1/6$.

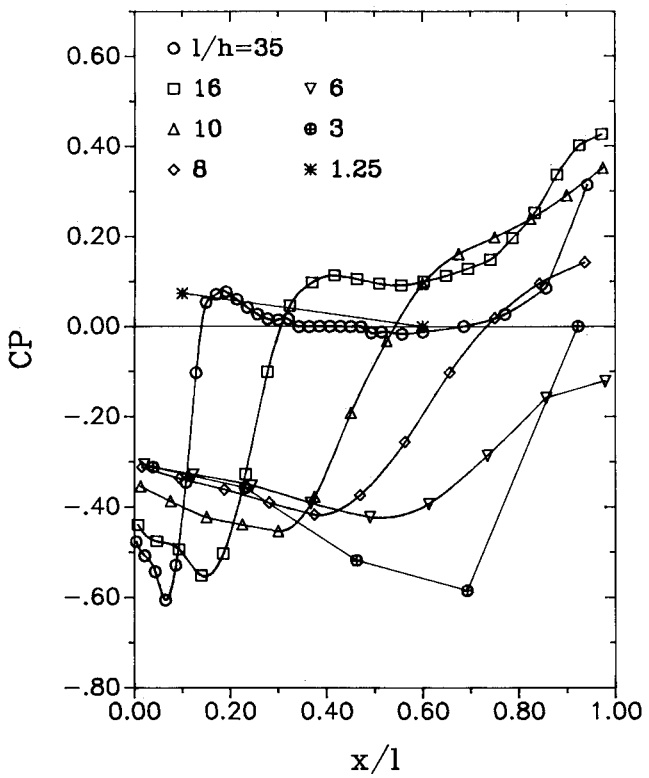

Fig. 5c Forebody pressure distributions, $h/d_2 = 1/3$.

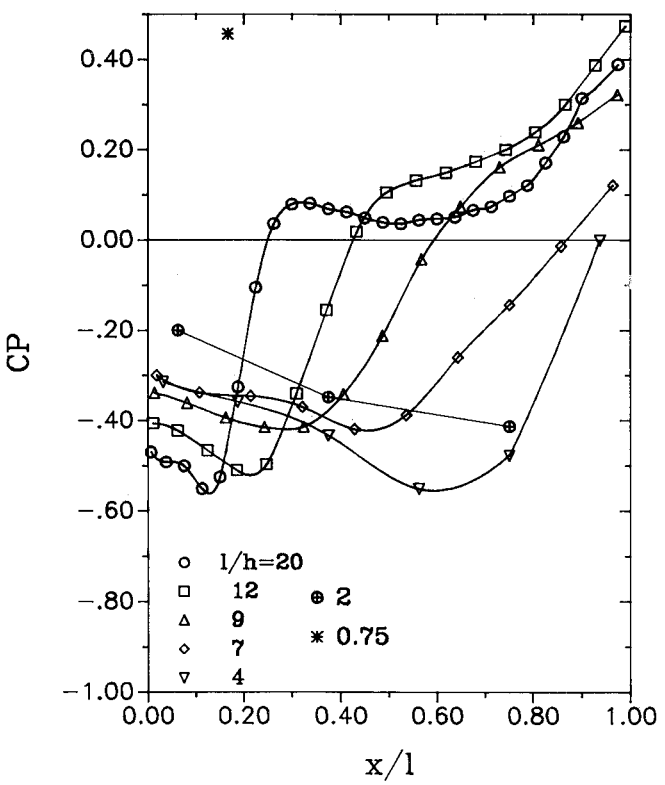

Fig. 5d Forebody pressure distributions, $h/d_2 = 1/3$.

other rings are larger but not so much as to make the separation and boundary-layer thicknesses totally negligible. It would be expected, then, that varying the ring height would influence the separated zone local to the ring in the closed mode and the entire separated zone in the open mode. However, the rings apparently are not large enough to significantly

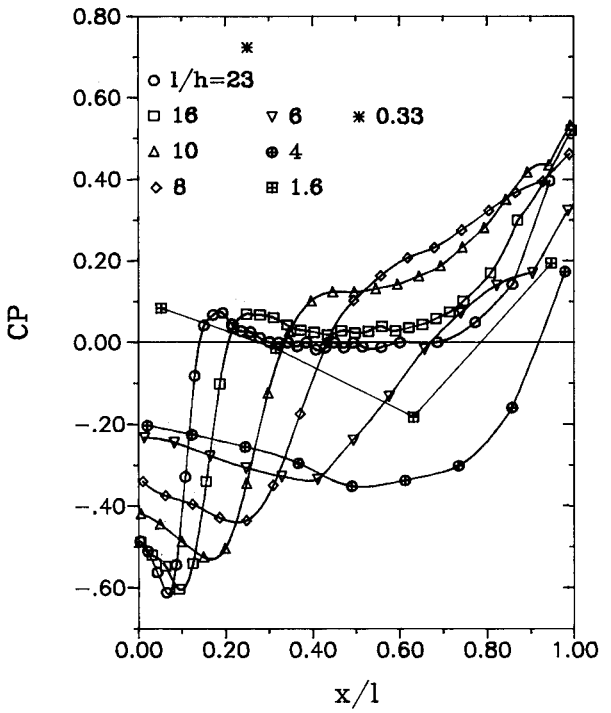

Fig. 5e Forebody pressure distributions, $h/d_2 = 1/2$.

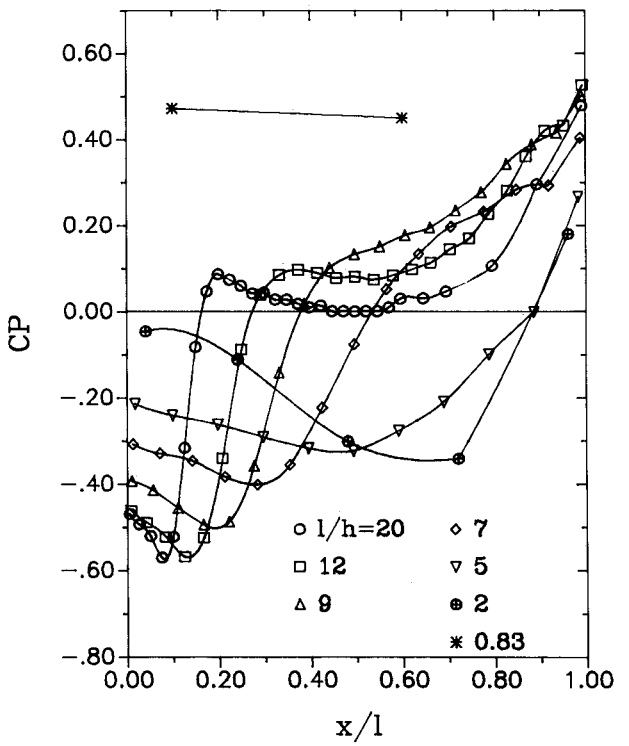

Fig. 5f Forebody pressure distributions, $h/d_2 = 1/2$.

alter the upstream separated zone in the closed mode, until the forebody length is reduced nearly to the transition length from closed to open flow.

Reattachment and Separation

This study is particularly concerned with defining the flow regions and modes that develop as the forebody aspect ratio (l/h) and the ring height ratio (h/d_2) are varied. Central to this concern are the locations of the reattachment and separation points. Two flow visualization techniques, tufts and oil

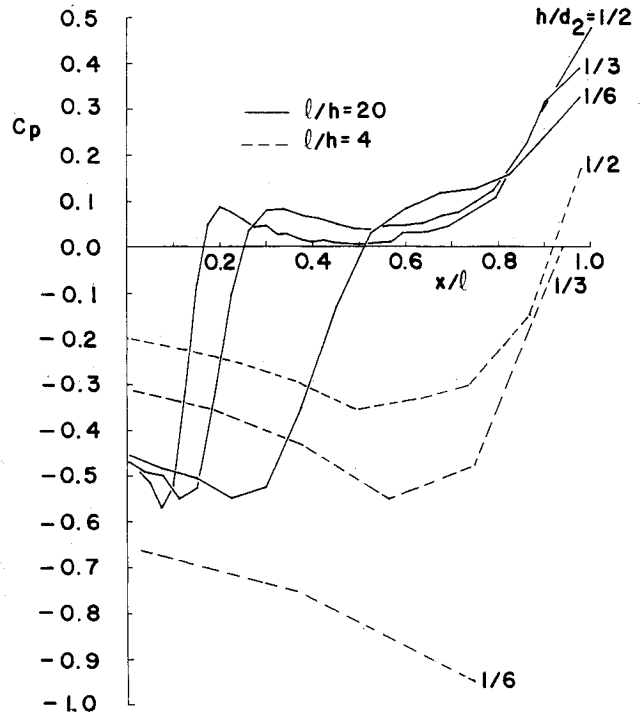

Fig. 6 Forebody pressure distributions for constant forebody aspect ratio ℓ/h; relative axial position, x/ℓ.

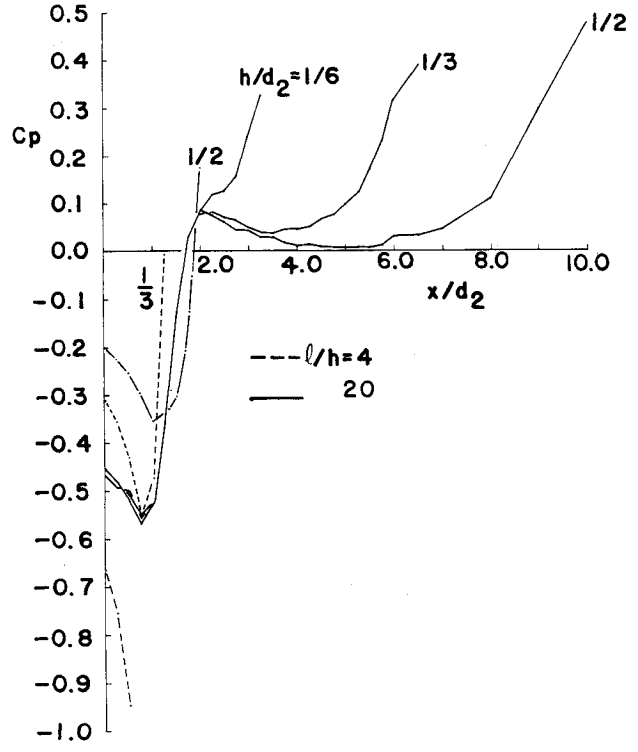

Fig. 7 Forebody pressure distributions for constant forebody aspect ratio, ℓ/h; absolute axial position, x/d_2.

flow, were used to find these points. In general, the two methods were in good agreement, especially for the reattachment points, although the tufts tended to indicate somewhat shorter separated zones. Because the tufts were more difficult to use and produced more uncertainty in the measured lengths than the oil, the results reported here are all from oil flow observations.

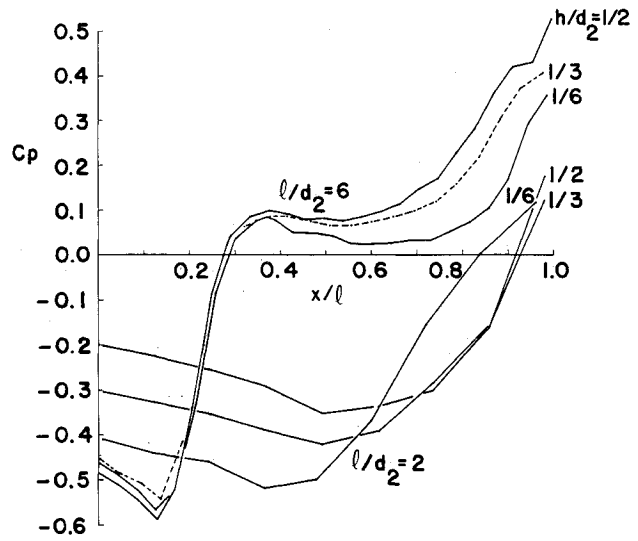

Fig. 8 Forebody pressure distributions for constant absolute forebody length, ℓ/d_2; relative axial position, x/ℓ.

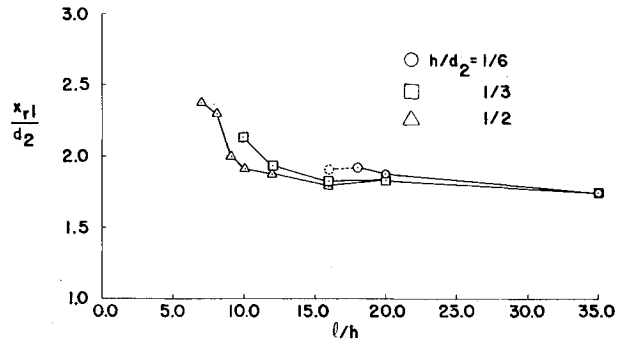

Fig. 9 Distance to reattachment downstream of the face, closed mode.

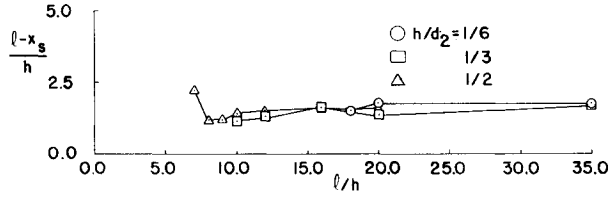

Fig. 10 Separation length ahead of the ring, closed mode.

If we refer to Fig. 1, there are three points of interest: the point x_{r1} at which the upstream separated closed mode flow reattaches to the forebody; the point x_s where the forebody flow separates ahead of the ring; and the point x_{r2} where the flow, for all modes, ultimately reattaches downstream of the ring. Although pressure distributions downstream of the ring have not been presented (in the interests of brevity), the downstream reattachment point is shown to indicate the nature of this region and also because it clearly reveals the three flow modes.

The closed mode forebody reattachment point, x_{r1} (which is also the reattachment length), is presented in Fig. 9 where it is normalized by the cylinder diameter. This normalization is chosen because, as was seen with the pressure distributions, the cylinder diameter dominates the upstream separated zone. At large values of l/h, the reattachment length is the same for all rings with a value of approximately 1.7. As l/h decreases, the reattachment length increases, but only very slowly at first.

Eventually, a point is reached, dependent on the ring height, at which the reattachment length increases more rapidly. The ring is now sufficiently close to the upstream separated zone to have an influence on that separation. Further decreasing l/h lengthens the reattachment until suddenly the reattachment point disappears.

The disappearance of x_{r1} signifies the transition from the closed mode to the open mode, and the forebody length at which x_{r1} disappears is accordingly defined as the critical length. With the techniques used here, it was difficult to ascertain precisely when x_{r1} disappeared, especially with the smallest ring, and so only estimated critical lengths can be given. These are $l/h = 16, 9, 6$ for $h/d_2 = 1/6, 1/3, 1/2$, respectively. In terms of l/d_2, the critical lengths are 2.67, 3, and 3 for $h/d_2 = 1/6, 1/3, 1/2$, showing that the absolute critical lengths are essentially the same. Interestingly, Ota observed that on a cylinder alone the skin friction and integral boundary-layer thicknesses had nearly recovered from the reattachment process at three diameters downstream from the cylinder face. It may be that transition from closed to open flow is instigated when the ring intrudes into that part of the boundary layer that is still recovering from reattachment.

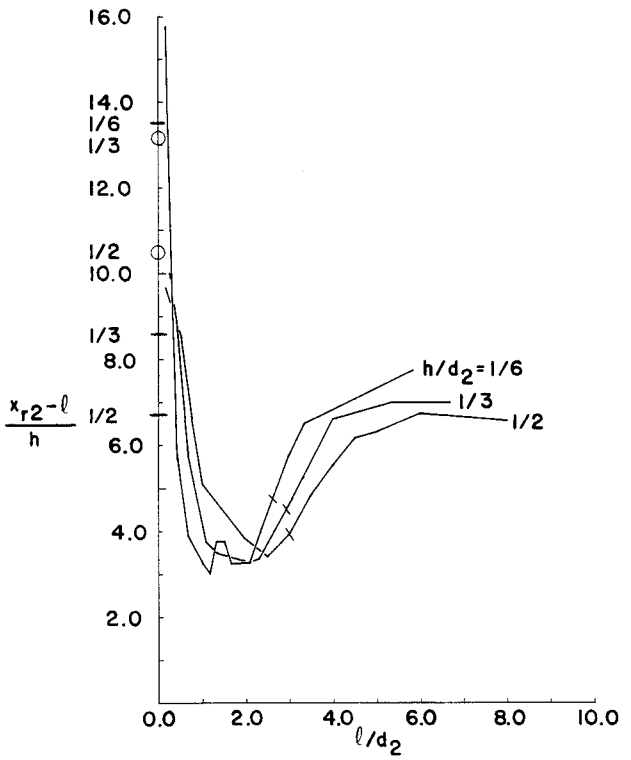

Fig. 11 Distance to reattachment downstream of the ring, all modes.

The downstream separated zone in the closed mode is characterized by its length, $l - x_s$, that appears in Fig. 10 normalized by the ring height. This normalization is chosen in response to the observation that the ring height dominates the flow local to the ring. From Fig. 10, there is generally little change in the length of the downstream separated zone as l/h changes. A nominal value of $(l - x_s)/h$ is 1.5 for all of the rings investigated. The largest ring shows a rapid increase in the zone length just before it disappears at the critical forebody length. The flow visualization gave a less distinct indication of separation than of reattachment, and very near the critical condition, it was particularly difficult to identify the separation point. Consequently, the rapid increase may occur for the other two rings as well, even though it was not observed.

The length of the separated zone behind the ring, $x_{r2} - l$, characterizes that region and is shown in Fig. 11 normalized by the ring height, again because the ring height should primarily govern the local flow. The abscissa is now l/d_2 rather than l/h. For large l/d_2, the length of the separation is roughly constant with a value dependent on the ring height. The distances to reattachment for the two larger rings at large l/d_2 are much nearer in value (7 and 6.5 ring heights for $h/d_2 = 1/3$ and $1/2$) than the smallest ring (8 heights). Since the two larger rings extend above the cylinder boundary layer, the boundary-layer influence on them is more nearly the same than it is on the smallest ring. Consequently, the reattachment lengths for the larger rings approximately scale with the ring height.

Decreasing l/d_2 produces a considerable decrease in the ring reattachment length to a minimum value of between 3 and 3.5 ring heights, followed by a very rapid and large increase in the distance to reattachment. Although there are detail differences between the three rings, generally the reattachment length downstream of the ring scales with the ring height. The diagonal marks appearing on the curves indicate the critical forebody length and show that the reattachment length begins to decrease well before the forebody mode changes. The numbered bars on the ordinate axis represent the distance to reattachment for a flat-faced cylinder with a diameter, $d_1 = d_2 + 2h$, that is the same as the ring diameter. When l becomes zero, it might be expected that the flow would resemble a flat-faced cylinder flow for which reattachment (x_{rcyl}) occurs at 1.7 diameters downstream. Then,

$$\lim_{l \to 0} \frac{x_{r2} - l}{h} = \frac{x_{rcyl}}{h} = \frac{x_{rcyl}}{d_1}\frac{d_1}{h} = 1.7 \times \frac{d_2 + 2h}{h}$$

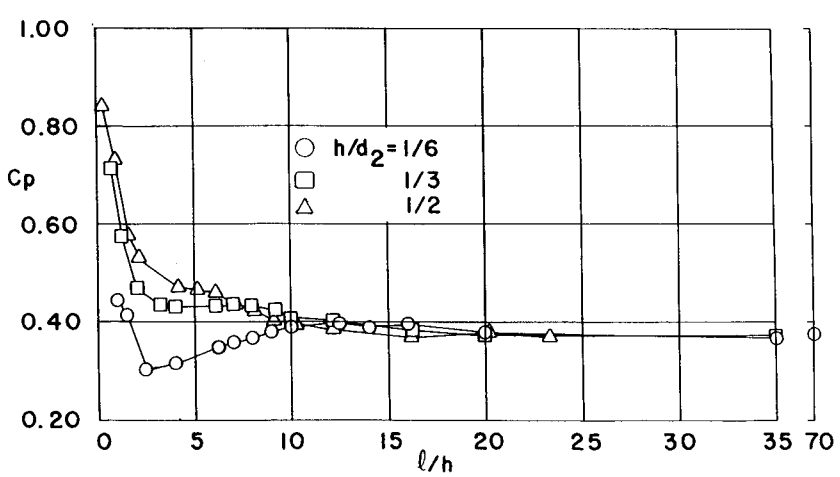

Fig. 12 Face corner pressure.

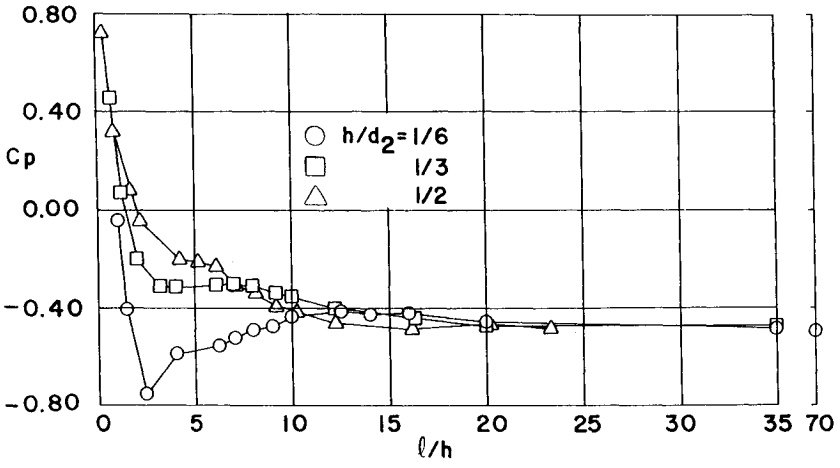

Fig. 13 Side corner pressure.

Clearly, the reattachment length is much greater than this limit. If the limiting case is treated as a disk of diameter d_1, then x_{r2} should approach the length at which the disk wake closes; that is, $x = 2.6$ diameters.[21] This length is indicated by the numbered circles on Fig. 11 and shows that cylinder/ring flow more closely resembles a disk flow as the forebody length goes to zero.

The rapid increase in reattachment length behind the ring that occurs near $l/d_2 = 1$ signifies the beginning of the third forebody mode. When the ring is relatively close to the cylinder face, the cylinder/ring arrangement begins to take on the appearance of a larger diameter disk with a protuberance on its face. The separation downstream of the ring then behaves more as a disk wake as previously noted.

Corner Pressure

Figures 12 and 13 isolate the pressures at the corner of the cylinder. The face corner pressure (Fig. 12) is measured at a radius $r/r_2 = 0.958$, whereas the side corner pressure (Fig. 13) is measured at $x/d_2 = 0.042$. These pressures show a gradual increase as l/h decreases through the closed-open transition, and then, for the two larger rings, the pressures rapidly increase as the forebody enters the disk mode. The small ring has a curious and unexplained decrease in these pressures before the disk mode develops. There appears to be a plateau in the open mode corner pressures for the two larger rings. A comparison of Figs. 12 and 13 shows clearly that the face and side corner pressures track each other quite precisely.

Conclusion

At least three distinct flow modes characterize the axisymmetric arrangement of a cylinder and ring in a low Mach number subsonic stream. Two modes are essentially the same as the closed and open modes observed with conventional rectangular cavities. The closed mode occurs for long cavities (or forebody lengths, here) and has two separated zones with a nominally constant pressure plateau between them. For shorter forebodies, the open mode with a single separated zone filling the cavity occurs. When the forebody length is very short, a third mode develops in which the forebody region more resembles a disk with a protuberance than a cylinder with a downstream disturbance.

Generally, details of the flow depend both on the forebody cavity aspect ratio, l/h, and the ring height ratio, h/d_2. The latter ratio reflects the significance of the thickness of the separated zone induced by the cylinder face and the subsequent reattaching and developing boundary layer on the cylinder side relative to the ring height. Two features that appear to be relatively independent of the ring height are the pressures in the upstream separated zone and the length of the downstream separated zone in the closed mode.

Pressure distributions and critical lengths for axisymmetric cavities in low-speed flow appear to be generally unavailable in the open literature. The results reported here should, therefore, be of use in situations involving axisymmetric cavitylike flow.

References

[1] Roshko, A., "Some Measurements of Flow in a Rectangular Cutout," NACA TN 3488, Aug. 1955.

[2] Charwat, A.F., Roos, J.N., Dewey, F.C. Jr., and Hitz, J.A., "An Investigation of Separated Flows—Part I: The Pressure Field," *Journal of the Aerospace Sciences*, Vol. 28, No. 6, June 1961, pp. 459–470.

[3] Tani, I., Tuchi, M., and Komoda, H., "Experimental Investigation of Flow Separation Associated with a Step or Groove," Aeronautical Research Institute, Univ. of Tokyo, Rept. 364, April 1961.

[4] Fox, J., "Surface Pressure and Turbulent Airflow in Transverse Rectangular Notches," NASA TN D-2501, Nov. 1964.

[5] Haugen, R.L. and Dhanak, A.M., "Momentum Transfer in Turbulent Separated Flow Past a Rectangular Cavity," *Transactions of ASME, Journal of Applied Mechanics*, Series E, Vol. 33, No. 3, Sept. 1966, pp. 641–646.

[6] Rossiter, J.E., "Wind-Tunnel Experiments on the Flow Over Rectangular Cavities at Subsonic and Transonic Speeds," ARC R & M 3438, 1966.

[7] McGregor, O.W. and White, R.A., "Drag of Rectangular Cavities in Supersonic and Transonic Flow Including the Effects of Cavity Resonance," *AIAA Journal*, Vol. 8, Nov. 1970, pp. 1959–1964.

[8] Wu, J.M., Chen, C.H., Moulden, T.H., Reddy, K.C., Collins, F.G., Nygaard, R., Kuwano, H., Vakili-Dast-Jud, A. and Sickles, W., "Fundamental Studies of Subsonic and Transonic Flow Separation: Part II—Second Phase Summary Report," AEDC-TR-77-103, Dec. 1977.

[9] Betry, M.R. and Rohrer, L.A., "Literature Survey of Aircraft Cavity Flow," AFWAL-TM-83-160-FIMM, May 1982.

[10] Johannsen, N.H., "Experiments on Supersonic Flow Past Bodies of Revolution with Annular Gaps of Rectangular Section," *Philosophical Magazine*, Series 7, Vol. 46, No. 372, Jan. 1955, pp. 31–39.

[11] Sarohia, V., "Experimental Investigation of Oscillations in Flows Over Shallow Cavities," AIAA Paper 76–182, Jan. 1976.

[12] Gharib, M., "The Effect of Flow Oscillations on Cavity Drag, and a Technique for Their Control," Ph.D. Thesis, California Institute of Technology, 1983.

[13] Koenig, K. and Roshko, A., "An Experimental Study of Geometrical Effects on the Drag and Flow Field of Two Bluff Bodies Separated by a Gap," *Journal of Fluid Mechanics*, Vol. 156, July 1985, pp. 167–204.

[14] Mason, W.T. Jr. and Beebe, P.S., "The Drag-Related Flow Field Characteristics of Trucks and Buses," in *Aerodynamic Drag Mechanisms of Bluff Bodies and Road Vehicles*, edited by G. Sovran, T. Morel, and W.T. Mason, Plenum, New York, 1978, pp. 45–94.

[15] French, N.J. and Jecmen, D.M., "Transonic/Supersonic Wind Tunnel Investigation of Effects of Parametric Variations in Nose Fairing and Aerospike Geometry on Trident 1 C4 Missile Body Static

Stability and Drag," Lockheed Missiles and Space Co., Sunnyvale, CA, LMSC-D 366908, Sept. 1974.

[16]Haupt, B.F., Buff, R.S., and Koenig, K., "Aerodynamic Effects of Probe-Induced Flow Separation on Bluff Bodies at Transonic Mach Numbers," AIAA Paper 85-103, Jan. 1985.

[17]Vincent, L.D., "Interacting Separated Flows," M.S. Thesis, Mississippi State University, Dec. 1984.

[18]Griffin, L.W., "An Experimental Study of Separated Flows Related to Blunt Body Drag Reduction Techniques," Mississippi State University, presented at the AIAA Southeastern Regional Student Conference, April 1985.

[19]Ota, T., "An Axisymmetric Separated and Reattached Flow on a Longitudinal Blunt Circular Cylinder," *Transactions of the ASME, Journal of Applied Mechanics*, Series E, Vol. 42, No. 2, June 1975, pp. 311-315.

[20]Stanbrook, A., "Experimental Pressure Distributions on a Plane-Nosed Cylinder at Subsonic and Transonic Speeds," ARC R and M No. 3425, 1966.

[21]Carmody, T., "Establishment of the Wake Behind a Disk," *Transactions of the ASME, Journal of Basic Engineering*, Series D, Vol. 86, No. 4, Dec. 1964, pp. 869-882.